Applied Catalysis B: Environmental 162 (2015) 180–186

Contents lists available at ScienceDirect

Applied Catalysis B: Environmental

journal homepage: www.elsevier.com/locate/apcatb

Local structure of vanadium in Ti-6Al-4V alloy anodized in acetic acid aqueous solution and its contribution to visible light response in photocatalysis

Yoshiteru Mizukoshi[a,*], Toshihiro Okajima[b], Naoya Masahashi[a]

[a] Kansai Center for Industrial Materials Research, Institute for Materials Research, Tohoku University, Gakuen-cho 1-2, Naka-ku, Sakai, Osaka 599-8531, Japan
[b] Kyushu Synchrotron Light Research Center, Yayoigaoka 8-7, Tosu, Saga 841-0005, Japan

ARTICLE INFO

Article history:
Received 27 March 2014
Received in revised form 20 June 2014
Accepted 26 June 2014
Available online 6 July 2014

Keywords:
Photocatalyst
Anodization
Titanium alloy
Visible light response
Vanadate

ABSTRACT

Anodization of Ti-6Al-4V alloy in acetic acid aqueous solution resulted in the formation of amorphous oxide on its surface; the amorphous oxide transformed into crystalline oxide primarily consisting of anatase TiO_2 by annealing. The annealed anodic oxide, especially those anodized in 1–2 mol L^{-1} acetic acid aqueous solution, could photocatalytically decompose acetaldehyde under visible light illumination. X-ray photoelectron spectroscopy, Raman spectroscopy, and X-ray absorption near-edge structure spectroscopy analyses showed that the vanadium is pentavalent and exists in an oxygen-tetragonal structure composed of VO_4^{3-} units. When the vanadate absorbs visible light, the excited electrons move into the conduction band of anatase TiO_2 so that recombination with holes was restricted. As a result, the anodic oxide exhibited superior photocatalytic activity under visible light illumination.

1. Introduction

About 40 years have passed since the first report by Honda and Fujishima on using TiO_2 as a photocatalyst [1]; however, practical uses and applications of the photocatalyst have been limited, contrary to expectation.

Improving the visible light response of the photocatalyst is one of the issues that need to be addressed. The band gap of TiO_2, the most widely studied photocatalyst, is 3.2 eV (corresponding to 388 nm) for the anatase phase or 3.0 V (413 nm) for the rutile phase. Solar light is a favorable excitation source for the photocatalyst; however, UV light makes up a small fraction of the solar spectrum. It is well known that doping modifies the band structure of the photocatalyst such that it absorbs at longer wavelengths when compared to pristine TiO_2 [2,3]. However, mass productivity and durability of the photocatalyst over long-term usage have not been achieved.

Another problem is the physical form of commercial photocatalysts, as most of them are supplied as a powder or a slurry, owing to which they need to be coated on suitable substrates prior to use. Unfortunately, the activities of coated photocatalysts are lower than those of pristine powder or slurry, mostly because of the decrease in the surface area. The long-term durability of the coated photocatalyst layers is also of concern.

To overcome these issues, we have prepared a TiO_2 photocatalyst by anodic oxidation of Ti and Ti alloy substrates. Anodic oxidation is well known as an easy method for surface modification of valve metals using simple equipment and is applicable to large and/or complex shaped substrates, which is advantageous for practical applications. In addition, anodized TiO_2 is expected to have high durability because of its high exfoliation strength. We previously reported the characteristics of a TiO_2 photocatalyst prepared by anodic oxidation [4,5]. In an electrolyte composed of aqueous sulfuric acid solution, the photocatalytic activities of sulfur-doped TiO_2 under visible light illumination were improved, probably due to narrowing of the band gap. More recently, we reported the anodic oxidation of Ti-6Al-4V (hereafter described as Ti64), which has been commonly used in Ti alloys having balanced workability and strength. When sulfuric acid was used as the electrolyte, the oxide was not formed homogeneously and the photocatalytic activities were poor [6], whereas an anodic oxide fabricated in acetic acid aqueous solution exhibited good photocatalytic activities even under visible light illumination [7].

* Corresponding author. Tel.: +81 72 254 6372; fax: +81 72 254 6375.
E-mail addresses: mizukosi@imr.tohoku.ac.jp (Y. Mizukoshi), okajima@saga-ls.jp (T. Okajima), masahasi@imr.tohoku.ac.jp (N. Masahashi).

http://dx.doi.org/10.1016/j.apcatb.2014.06.050
0926-3373/

In the present study, we investigated the characteristics of an anodic oxide prepared in a range of acetic acid concentrations and its detailed structure to clarify the origin of the visible light response.

2. Experimental

2.1. Materials

A Ti64 hot-rolled thin plate with a thickness of 1 mm was supplied by Titan-Meister (Sendai, Japan). Acetic acid and acetaldehyde were purchased from Wako Pure Chemicals (Japan) and used without further purification. Water used in the present study was purified by a water purifier (Ul-pure; Komatsu Electronics) containing a reverse osmosis membrane, an ion exchange column, and photocatalytic TOC (total organic carbons) removal processes. The purity of the He carrier gas for GC analyses was 99.999%.

2.2. Anodization

A Ti64 plate (cp-Ti, grade I) with dimensions of $19 \times 9 \times 1\ mm^3$ was used as the anode. It was polished using SiC grinding paper of 1500 grit, followed by rinsing in ethanol in an ultrasonic cleaner and drying in air. The anodizations were conducted for 30 min using a DC power supply (Matsusada Precision, PRk 500-3.2, Japan) in an acetic acid aqueous solution whose concentration ranged from 0.01 to 6 mol L^{-1}. A Pt mesh electrode ($5 \times 5\ cm^2$) was used as the cathode. The anodized Ti64 was rinsed with pure water, dried, and annealed at 723 K for 5 h in an air atmosphere. Hereafter, the anodized and anodized/annealed Ti64 are denoted as "Ti64_as" and "Ti64_an", respectively.

2.3. Characterization

2.3.1. XRD

The crystallographic structure of the anodic oxide was determined by X-ray diffraction (PANalytical X'Pert diffractometer, Netherlands) with CuKα radiation (0.15406 nm) at a scan rate of $1^\circ\ min^{-1}$ and a rotating detector. The sample was set in a thin-film geometry arrangement with a glancing angle of 0.5°.

2.3.2. SEM observations

Microstructure observations were conducted with a scanning electron microscope (Keyence VE-8800, Japan) at an operating voltage of 20 kV.

2.3.3. XPS measurements

X-ray photoelectron spectroscopy (XPS) measurements were carried out with an electron spectrometer (Kratos AXIS-Ultra DLD, Shimadzu, Japan) equipped with monochromated Al Kα radiation at a base pressure of 3.0×10^{-7} Pa. The photoelectron take-off angle (TOA) was set at 90°, where TOA is defined as the angle between the substrate surface and spectrometer slit.

2.3.4. Spectroscopic measurements

Diffuse reflectance spectra and the corresponding chromaticity parameters for CIELab*, developed by CIE (Commission Internationale d'Eclairage), were obtained using a UV–vis spectrophotometer (Jasco V-550, Japan).

Chemical states and distributions of Ti, Al, and V on the surface of the anodic oxide were investigated using a Raman microscope (inVia, Renishaw, UK). The wavelength of the excitation laser was 532 nm. An area of $220.8 \times 132.6\ \mu m$ was analyzed with a step size $3.2 \times 2.6\ \mu m$. The total number of sampling points was 3519.

2.3.5. Determination of dissolved elements during the anodization

Ti, Al, and V dissolved in the electrolyte during the anodization were determined by an induced coupled plasma (ICP) emission spectrometer (Shimadzu. ICPE-9000). Residue formed during the anodization was dissolved in hot concentrated sulfuric acid prior to the ICP analyses.

2.3.6. XANES measurements

V and Ti K-edge X-ray absorption near-edge structure (XANES) spectra were measured at beam line BL11 of the Kyushu Synchrotron Light Research Center in convergent electron yield (CEY) mode for the Ti64 plates before and after anodization and in transmission mode for reference samples [8]. Theoretical V K-edge XANES spectra were also obtained with generalized gradient approximation (GGA) using full-potential augmented plane wave plus local orbitals (APW + lo) calculations [9]. The core-hole effects were taken into account in these calculations. The theoretical spectral profiles were obtained as a product of the radial part of the transition matrix element and the corresponding projected partial density of states. Each calculated spectrum was broadened by a Gaussian function of $\Gamma = 1.0$ eV full width at half maximum.

2.4. Photocatalytic activities

The photocatalytic activities were evaluated by monitoring the decomposition of acetaldehyde in air. Acetaldehyde (50 μL, 900 μmol) was introduced into a cylindrical Pyrex glass vessel with a quartz window. Prior to the introduction of acetaldehyde, illumination by an ultra-high-pressure Hg lamp (SX-UI501HQ, Ushio, Japan) was used to remove the residual organic species, originating from acetic acid, until no CO_2 evolution was observed. Light illumination was conducted with a Xe lamp (MAX-302, Asahi Spectra, Japan) equipped with optical filters. When a 365-nm band pass filter and 400- and 422-nm shorter wavelength cut-off filters were employed, the illuminated light intensities were 1.1, 91.2, and 88.5 mW cm^{-2}, respectively. The decomposition products were determined by GC (GC-2014, Shimadzu, Japan). The amounts of CO_2 evolution were calibrated against the CO_2 evolved in the blank test when acetaldehyde was exposed to light in the absence of the TiO_2 photocatalyst.

3. Results and discussion

3.1. Anodization

Fig. 1 shows the time profiles of applied voltage, applied current, and the ratio of voltage to current during the anodization of the Ti64 substrate in acetic acid electrolyte of varying concentrations. The pH and conductivity of the electrolyte are also shown in the figure.

At low concentrations of acetic acid, the voltage promptly reached the pre-set value of 210 V. However, the current gradually decreased because the pre-set current of 200 mA could not be maintained at a voltage of 210 V. In the cases of 0.05 and 0.2 mol L^{-1} of acetic acid, the current became zero within 30 min of the anodization, longer than the time taken for Ti anodization in acetic acid electrolyte at the same concentrations [10]. This is attributable to the low conductivity of the electrolyte and the electrical resistance of the formed oxide layer. The longer time taken to reach zero current suggests a thin and/or less dense structure of the anodic oxide, possibly due to the dissolution of the alloy elements during anodization. For example, Zwilling et al. reported that V dissolved during anodization of Ti64 [11].

When the acetic acid concentration is 1 or 2 mol L^{-1}, a longer time was required to reach the pre-set voltage, and the current decreased but did not become zero during the 30 min of the

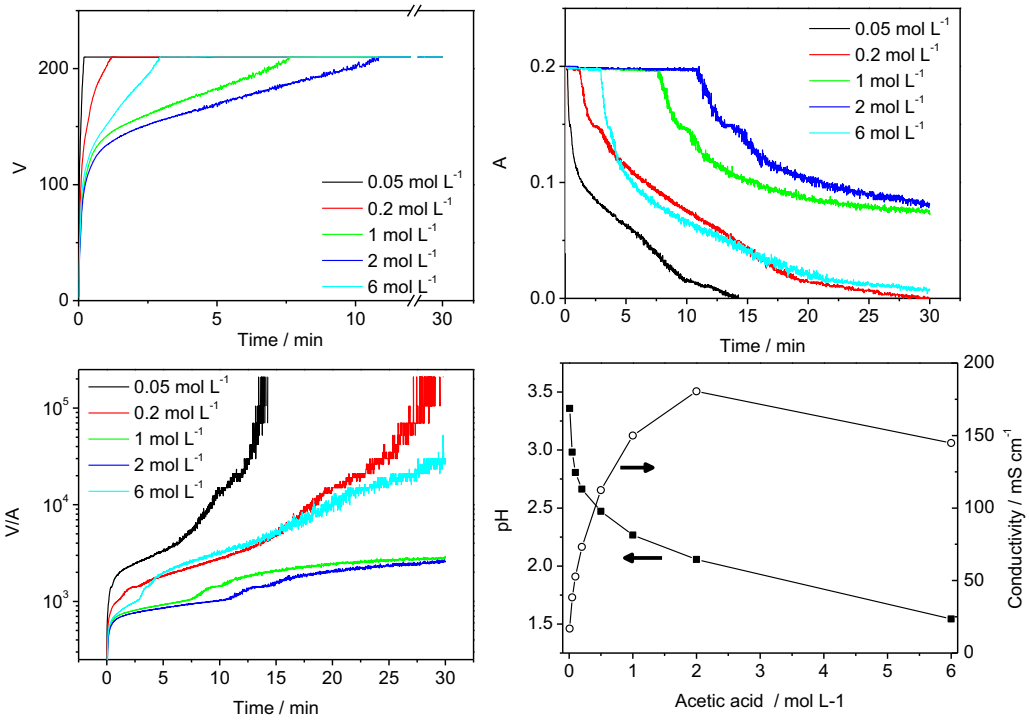

Fig. 1. Time profiles of (a) applied voltage, (b) current, and (c) the ratio of voltage to current. (d) pH and conductivity at various concentrations of acetic acid aqueous solution.

anodization. The apparent resistance, calculated from the applied voltage and current, is smaller in 1–2 mol L^{-1} acetic acid than it is in 0.05–0.2 mol L^{-1}. This cannot be explained only from the conductivity of the electrolyte and is thought to originate from the nature of the fabricated oxide, including its morphology (see section 3.3). At even higher concentrations, e.g., 6 mol L^{-1}, the electric profiles are similar to that at 0.2 mol L^{-1}.

3.2. Spectral feature of the anodic oxide

The color of the anodized sample varies with the concentration of acetic acid in the electrolyte and with the annealing or not. Differing from the anodization of Ti64 in sulfuric acid electrolyte, the surface is homogeneously colored in acetic acid.

Fig. 2 shows the absorption spectra of the anodic oxides. Spectra were transformed into Kubelka-Munk units. The as-anodized sample does not absorb in the visible light region. On the other hand, the annealed samples absorb in the visible region, at wavelengths shorter than about 510 nm. The absorption edge, which is characteristic for a semiconductor, is not observed in the spectrum of 0.2 mol L^{-1} acetic acid, because the residual metallic luster, indicative of the thin oxide layer, hindered the measurement of the diffuse reflectance spectra. In the cases of 1 and 2 mol L^{-1} acetic acid, absorption in the visible region definitely increases. In addition, the bend in the curve around 360 nm suggests an indirect transition. Contrary to this, the spectrum of Ti64 anodized in 6 mol L^{-1} acetic acid shows a lower intensity than those for Ti64 anodized in 1 and 2 mol L^{-1} acetic acid.

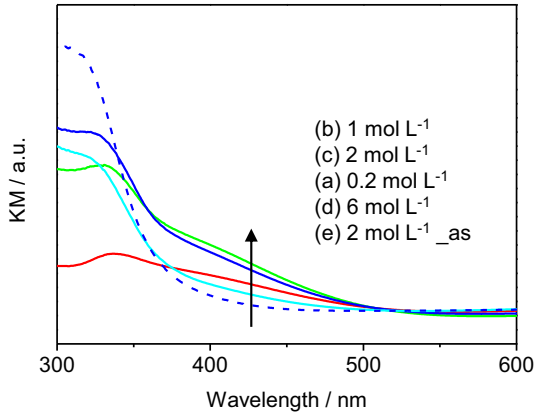

Fig. 2. Diffuse reflectance spectra of anodized Ti64 in (a) 0.2, (b) 1, (c) 2 and, (d) 6 mol L^{-1} acetic acid aqueous solution followed by annealing, and (e) as-anodized in 2 mol L^{-1} acetic acid.

The chromaticity parameters were obtained from the absorption spectra. The color of a substance corresponds to the wavelength of light reflected by it, and it can be expressed by three coordinates, namely, L^*, a^*, and b^*, where L^* is the lightness of color of an object ($L^* = 0$ indicates absolute black and $L^* = 100$ indicates absolute white), a^* is the degree of red/green, and b^* is the degree of yellow/blue. These coordinates are calculated by analyzing absorption spectra, and those of the anodized and annealed samples were plotted against the acetic acid concentration in the electrolyte in Fig. 3. For comparison, the results of the Ti substrate are also plotted. L^* for both substrates is almost the same. Regardless of acetic acid concentration, both a^* and b^* of Ti are almost zero, meaning that Ti anodized in acetic acid and annealed is colorless. On the other hand, the a^* and b^* values of Ti64 are negative and positive, respectively. The absolute values of a^* and b^* show their minimum and maximum values when the acetic acid concentration is between 1 and 2 mol L^{-1}. The dependence of acetic acid concentration coincides with the spectral features in Fig. 2.

3.3. SEM observation

The surface morphologies of the anodic oxide were observed by SEM (Fig. 4). In the case of 2 mol L^{-1} acetic acid, pores with diameters of several micrometers are formed, but the frequency of their formation is low and the surface is totally rough (Fig. 4 (a)). This is different from the surface of Ti64 anodized in sulfuric acid

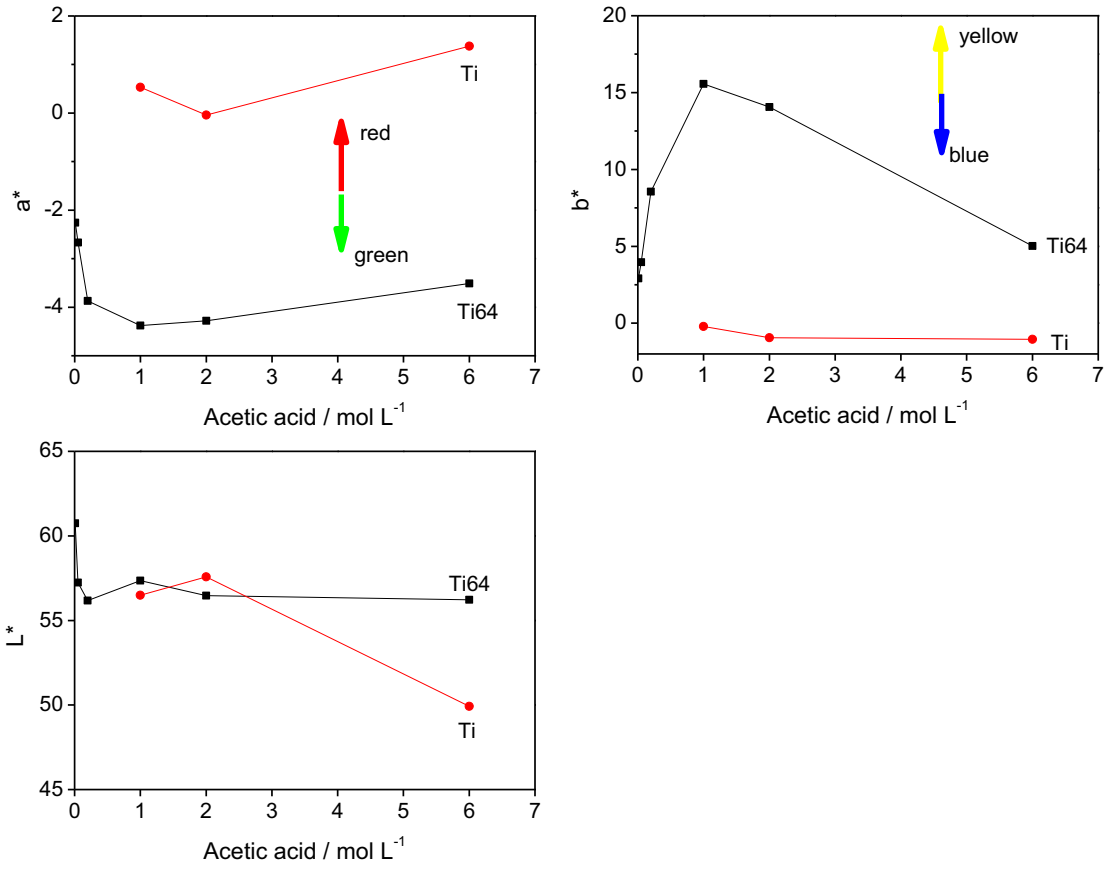

Fig. 3. CHE Lab* parameters of Ti_an and Ti64_an.

electrolyte [6], but similar to the surface of Ti anodized in acetic acid electrolyte [11]. The rim of the pore is pushed up (Fig. 4 (b)). At high magnification, the surface of the oxide appears to be an aggregate of small units on the order of sub-micrometers (Fig. 4 (c)). Post annealing, the surface morphology, including the pore sizes, is almost the same as that of the oxide before annealing, except for the observation of some cracks (Fig. 4 (d)). We consider that the inhomogeneous thickness due to the outstanding

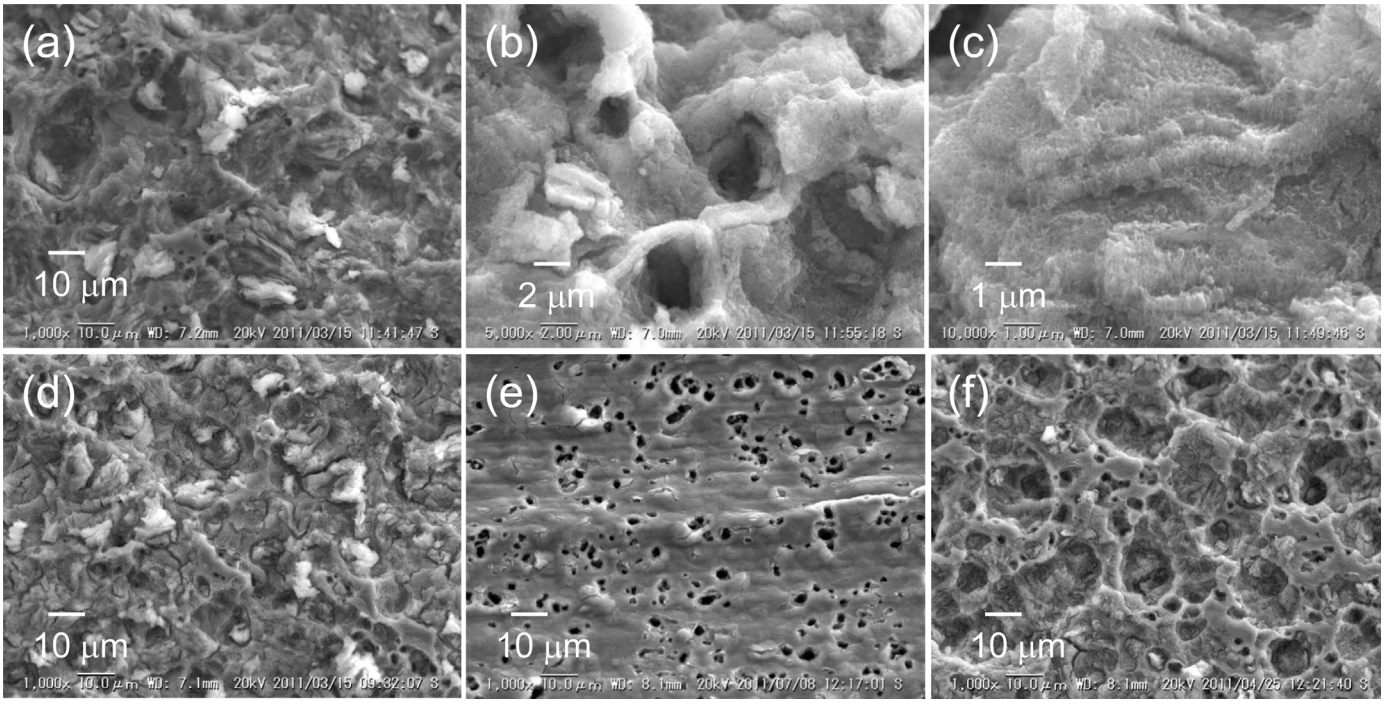

Fig. 4. SEM images of Ti64 anodized in 2 mol L^{-1} (a–d), 0.5 mol L^{-1} (e), and 6 mol L^{-1} acetic acid (f). (a–c) are as-anodized, and (d–f) are anodized and annealed samples.

Table 1
Compositions of anodic oxide surface, electrolyte solution, and residue after anodization.

	2 mol L^{-1} acetic acid			0.1 mol L^{-1} sulfuric acid		
	Oxide surface (at%)	Electrolyte solution (μmol L^{-1})	Residue (μmol L^{-1})	Oxide surface (at%)	Electrolyte solution (μmol L^{-1})	Ti64 substrate (at%)
Ti	24.7	182.0	7901	19.4	19.5	86.2
Al	3.0	32.4	866.5	6.1	4.9	10.2
V	2.5	12.8	320.1	0.5	4.6	3.6
Al/Ti[a]	1.0	1.5	0.9	2.7	2.1	1.0
V/Ti[a]	2.5	1.7	1.0	0.6	5.7	1.0

[a] Normalized values using the ratios of Ti64 raw substrate as standard.

surface roughness contributes to decrease the apparent resistance.

When the concentration of acetic acid is low (Fig. 4 (e)), the frequency of the pore formation is high, and the sizes and shapes are varied. Polishing flaws in the horizontal direction indicate that the oxide layer is not thick at this concentration. The surface roughness is not outstanding. At a high concentration of acetic acid (Fig. 4 (f)), the surface roughness decreases, resulting in a surface morphology similar to that for anodization at low concentration although the pore size is larger.

3.4. XRD

As previously reported, diffraction peaks assignable to oxides were not detected in the measurements of as-anodized Ti64 [7]. Fig. 5 shows diffraction patterns of the anodized and annealed samples. Regardless of acetic acid concentration, we observed peaks from anatase TiO_2. In contrast to Ti anodization in acetic acid, rutile TiO_2 was not detected [11]. The peak intensity of anatase TiO_2 is highest when the acetic acid concentration is 2 mol L^{-1}. In addition, oxides of Al and V were not detected in the XRD measurements, suggesting that the amount of crystalline oxide of Al or V is not large enough to result in diffraction peaks, or that they are amorphous.

3.5. Photocatalytic activity

The CO_2 evolution rates from photocatalytic decomposition of acetaldehyde are shown in Fig. 6. The annealed anodic oxides were employed in the evaluation because the as-anodized samples exhibited very poor activity [7]. Under the illumination of ultraviolet light (365 nm), the evolution rate is almost constant, regardless of the concentration of acetic acid. When visible light was used, the photocatalytic activities varied with the concentration of acetic acid. We observed a decline in the activity when the acetic acid concentration was too high or too low.

The visible light response is believed to originate from the Al or V compounds formed during the anodization. Therefore, further detailed analyses were conducted using Ti64, anodized in 2 mol L^{-1} acetic acid and annealed, as a typical sample.

3.6. Surface composition of oxide and dissolution of alloy components into electrolyte

The components of the top surface of the anodic oxide were also determined from XPS measurements. The results are given in Table 1. Some components of the Ti64 alloy are dissolved into the acetic acid electrolyte. The concentrations of Ti, Al, and V in the electrolyte after the anodization were measured by ICP, and the results are included in the table. The residue formed during anodization was also analyzed by ICP after the dissolution in hot concentrated sulfuric acid. In the case of 2 mol L^{-1} acetic acid, the V/Ti ratio at the top surface of the anodic oxide is 2.5 fold higher than that of the raw substrate, indicating that V is concentrated at the top surface during anodization and/or annealing. Zwilling et al. reported that TiO_2 and Al_2O_3 were formed at a Ti/Al ratio of about 5 during the anodization of Ti64 in chromic acid solution [11]. In their experiments, the amount of V in the oxide was determined to be small. In contrast, we observe that V is enriched at the surface of the anodic oxide, and its oxidation state is pentavalent, according to XPS results [7].

3.7. Raman spectroscopy

To investigate the chemical states of Ti, Al, and V, the surface of the anodized and annealed Ti64 was observed by a Raman microscope. A typical Raman spectrum is shown in Fig. 7 (a). Definite peaks at 155, 409, 521, and 641 cm^{-1} are assignable to E_g, B_{1g},

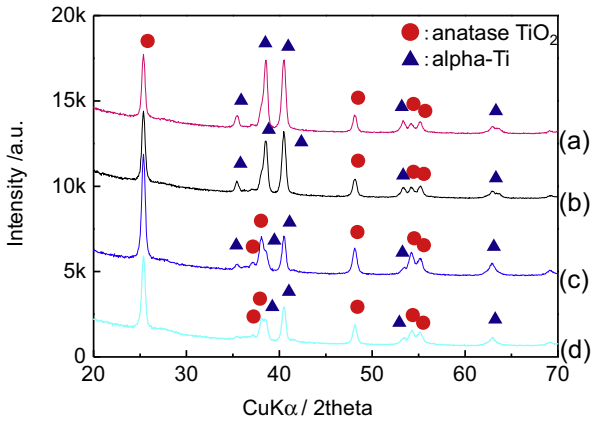

Fig. 5. XRD patterns of Ti64 anodized in (a) 0.01, (b) 0.05, (c) 2, and (d) 6 mol L^{-1} acetic acid and annealed.

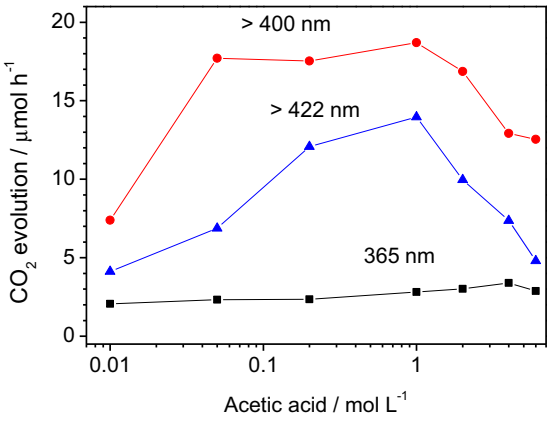

Fig. 6. Dependence of CO_2 evolution rates, from acetaldehyde photocatalysis, on the acetic acid concentration used as electrolyte during the anodization.

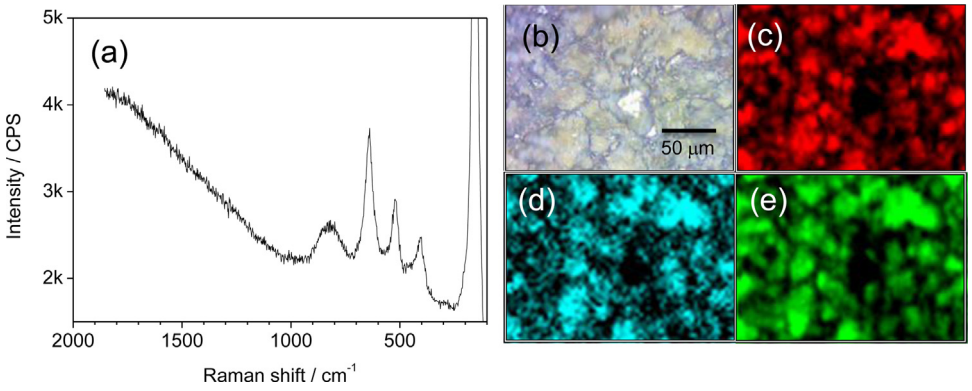

Fig. 7. (a) Raman spectrum of Ti64_an and planar distributions of the signal intensity of (c) 641, (d) 830 and (e) 1800 cm^{-1} in the selected area (b).

$A_{1g} + B_{1g}$, and E_g of anatase TiO_2, respectively [12,13]. The sharpness of these peaks indicates the high crystallinity of the fraction. It is reported that Al oxide does not show any Raman spectral features in the 100–1000 cm^{-1} region [14]; therefore, the rise in fluorescence background for wavenumbers beyond 1000 cm^{-1} is thought to be from Al_2O_3. No characteristic peaks originating from V_2O_5 (997, 700, and 485 cm^{-1}) are observed in the present spectrum [15]. Taking into account that V is pentavalent, another possibility for the chemical state of V is that it is a vanadate such as VO_4^{3-} and $V_2O_7^{4-}$. For example, $BiVO_4$ and $Mg_2V_2O_7$ exhibit Raman peaks at 826 and 838 cm^{-1}, respectively [16], which are located near the broad peak around 830 cm^{-1} in the present spectrum. The broadness of the peak suggests that it originates from a material of low crystallinity.

Planar distributions of the Raman signal intensity at 641, 830, and 1800 cm^{-1} (Fig. 7 (c)–(e)), which are assignable to anatase TiO_2, vanadate, and Al_2O_3, respectively, are obtained by scanning the designated area (Fig. 7 (b)). Al and V are used to stabilize the alpha- and beta-Ti phases during the fabrication of the Ti64 alloy. The distributions of Al and V are almost the same as the distribution of Ti, but the domains reflected from the vanadates are smaller than those of the others.

3.8. XANES spectroscopy

The measured Ti K-edge XANES spectra of the Ti64 substrate, Ti64_as and Ti64_an, are shown in Fig. 8 (a). The Ti K-edge spectra measured from some reference materials (anatase TiO_2, rutile TiO_2, Ti_2O_3, and Ti foil) are also shown in the figure. The spectral features of the Ti64 substrate before and after anodization are quite different, and are similar to those of Ti metal and anatase TiO_2, respectively. These results show that the Ti metal in the Ti64 alloy is oxidized to anatase TiO_2 by anodization and that the Ti in Ti64_an has an oxygen-octahedron structure with an oxidation number of +4. The characteristic pre-edge shape of Ti64_as is similar to the XANES spectrum reported by Matsuo et al., suggesting that Ti64_as contains amorphous TiO_x [17]. In the previous study, it was assumed that a Ti oxide fraction with low crystallinity was contained in Ti64_as due to the absence of the X-ray diffraction peaks from TiO_2, which is consistent with the present XANES results [7].

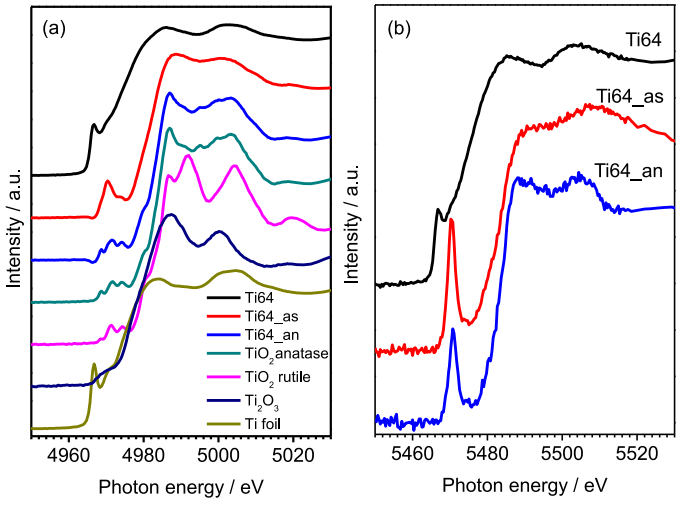

Fig. 8. (a) Ti K-edge XANES and (b) V K-edge XANES spectra of Ti64. Some Ti materials are also shown as references (a).

Fig. 8 (b) shows the V K-edge XANES spectra of raw Ti64, Ti64_as, and Ti64_an. Compared with raw Ti64, spectral changes in the anodized samples indicate the oxidation of V, but the spectral features are different from the reported spectra of VO_2, V_2O_3, and V_2O_5 [18]. The spectrum of Ti64_an is shifted in the high-photon-energy direction in comparison with the reference spectrum of VO_2/SiO_2 (not shown in the figure), supporting the pentavalence of V, determined by XPS measurements. Large pre-edge peaks were observed in the anodized samples, suggesting that V^{5+} found in the anodic oxide has low symmetry [19].

To clarify the local structure of V, we compared the measured XANES spectrum with simulated spectra. Fig. 9 (b) shows the calculated V K-edge XANES spectrum for the V substitutional model. In the model (shown in the inset), one Ti^{4+} ion in the $2 \times 2 \times 1$ supercell of an anatase-type TiO_2 unit cell is substituted by a V^{5+} ion. The V ion is 6-fold coordinated with O ions in the alloy. Comparing the V K-edge region between the anodized Ti64 alloy and the calculated result, we found the spectral features at around 5490–5510 eV to be roughly similar. However, definite differences are observed in the pre-edge region, at around 5470 eV in both spectra. This result shows that the V substitutional model is not suitable to explain the local structures of V ions in Ti64_an.

Walter et al. reported the V K-edge spectra of $Mg_2V_2O_7$, where V is located in an oxygen-tetrahedral structure [20]. The simulated spectrum of $Ti_2V_2O_7$ is shown in Fig. 9 (c). In this structure, the V ion is 4-fold coordinated with O ions. The shape of the pre-edge also matches that of the experimental one. Thus, the oxygen-tetrahedral model consisting of a VO_4 unit can suitably explain the local structure of V in Ti64_an. This model is also supported by Raman measurements, which show that the local structure of V is a vanadate such as VO_4^{3-} or $V_2O_7^{4-}$.

3.9. Band structure and visible light response

According to the results obtained using the above methods, the anodic oxide in this study is found to consist of anatase TiO_2,

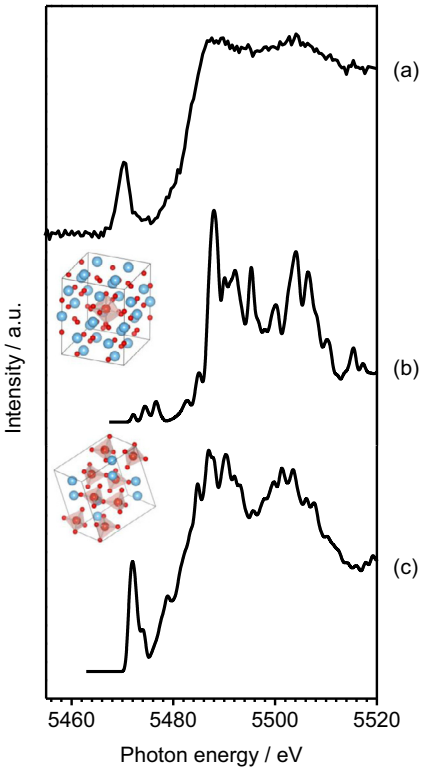

Fig. 9. Comparison of (a) the observed V-K edge XANES spectrum with the simulated spectra of (b) oxygen-octahedral and (c) oxygen-tetragonal local structures for V. Insets represent the structural models used for the simulations, where the blue and small and large red spheres denote Ti atoms, O atoms, and V atoms, respectively. (For interpretation of the references to color in this figure legend, the reader is referred to the web version of the article.)

vanadate (VO_4^{3-} or $V_2O_7^{4-}$), and Al_2O_3. Among these species, it is thought that Al_2O_3 cannot contribute to the improvement in the visible light response because of its wide band gap [21]. In the anodization of Ti64 in sulfuric acid aqueous solution, Al was localized near the surface of the oxide, shading the oxide surface, so that the photocatalytic activity of the formed oxide was low [6]. The composition of the anodic oxide and electrolyte when Ti64 was anodized in 0.1 mol L^{-1} sulfuric acid is also shown in Table 1. Compared with the anodization in acetic acid, a large amount of Al is located on the surface of the oxide. In contrast, a large quantity of V is dissolved into the electrolyte, and the amount remaining on the oxide is small. Taking this difference into account, it is reasonable to conclude that the superior photocatalytic activity of Ti64_an under visible light, observed in the present study, is derived from V.

Kudo et al. reported that the visible light response of a monoclinic $BiVO_4$ photocatalyst was derived from the transition from a valence band, formed by Bi 6s or a hybrid orbital of Bi 6s and O 2p, to a conduction band of V 3d; the energy of this band gap was estimated to be 2.4 eV [22], which is in good accordance with the band gap energy in the present case, estimated to be ca. 2.4 eV from UV–vis spectra [7]. Their theoretical calculations on Ag-ion-containing vanadate also showed that hybridization of O 2p and Ag 4d resulted in a new valence band, contributing to narrowing of the O $2p^-$ V 3p band gap [23]. On the other hand, Xiao et al. studied the photocatalytic activities of an $InVO_4$/anatase TiO_2 composite [24]. The composite photocatalyst showed photocatalytic activity when illuminated with light of wavelength shorter than 540 nm, which was reported to be due to the photosensitization of $InVO_4$. Their theoretical calculations showed that the energy level of O 2p in VO_4^{3-} was located at 1.0 eV more negative than that of the O 2p in anatase TiO_2. Consequently, $InVO_4$ with a narrowed bandgap absorbs visible light and generates photoelectrons, which move from the conduction band of VO_4 to the conduction band of TiO_2.

4. Conclusions

The good photocatalytic activity of the anodic oxide of Ti64, fabricated in acetic acid electrolyte, under visible light is derived from the localization of vanadate species on the surface of the oxide. The vanadate species serves as a visible light sensitizer. On the other hand, the anodic oxide prepared in sulfuric acid electrolyte shows poor activity because the oxide surface contains a lot of Al_2O_3, which shades the photocatalytic components below this layer owing to its broad band gap. These facts indicate that the structure of the anodic oxide, including the surface components, greatly depend on the anodization procedure used. In future work, we will investigate the formation mechanism of the anodic oxide of Ti alloy, focusing on the transfer of the constituents during anodization.

Acknowledgements

The authors wish to thank Ms. Y. Matsuda from IMR, Tohoku University, for preparing samples and evaluating photocatalytic activities, Mr. S. Sugiyama from IMR, Tohoku University, for preparing the Ti64 substrates, Ms. K. Ohmura from IMR, Tohoku University, for XPS analyses, Dr. J. Kugai from Osaka University for ICP analyses, and Shimadzu Co., Ltd., for their helpful assistance with Raman microscopy measurements. This study was partially supported by the Izumi Science and Technology Foundation.

References

[1] A. Fujishima, K. Honda, Nature 238 (1972) 37–38.
[2] R. Asahi, T. Morikawa, T. Ohwaki, K. Aoki, Y. Taga, Science 293 (2001) 269–271.
[3] M. Anpo, M. Takeuchi, J. Catal. 216 (2003) 505–516.
[4] N. Masahashi, Y. Mizukoshi, S. Semboshi, N. Ohtsu, Appl. Catal. B Environ. 90 (2009) 255–261.
[5] Y. Mizukoshi, N. Ohtsu, S. Semboshi, N. Masahashi, Appl. Catal. B Environ. 91 (2009) 152–156.
[6] N. Masahashi, Y. Mizukoshi, S. Semboshi, K. Ohmura, S. Hanada, Thin Solid Films 520 (2012) 4956–4964.
[7] Y. Mizukoshi, N. Masahashi, Chem. Lett. 41 (2012) 544–545.
[8] T. Okajima, K. Sumitani, M. Kawamoto, E. Kobayashi, J. Phys. Conf. Ser. 430 (2013) 012088 (6 pp).
[9] P. Blaha, K. Schwarz, G. Madsen, D. Kvasnicka, J. Luitz, WIEN2k, An Augmented Plane Wave +Local Orbitals Program for Calculating Crystal Properties, Karlheinz, Achwarz, Technical Universitat Wien, Austria, 2001.
[10] Y. Mizukoshi, N. Masahashi, Surf. Coat. Technol. 240 (2014) 226–232.
[11] V. Zwilling, E. Darque-Ceretti, A. Boutry-Forveille, D. David, M.Y. Perrin, M. Aucouturier, Surf. Interface Anal. 27 (1999) 629–637.
[12] H. Berger, H. Tang, F. Kevy, J. Cryst. Growth 103 (1993) 108–112.
[13] Z. Miao, D. Xu, J. Ouyang, G. Guo, X. Zhao, Y. Tang, Nano Lett. 2 (2002) 717–720.
[14] M.A. Vuurman, I.E. Wachs, J. Phys. Chem. 96 (1992) 5008–5016.
[15] G.C. Bond, S.F. Tahir, Appl. Catal. 71 (1991) 1–31.
[16] F.D. Hardcastle, I.E. Wachs, J. Phys. Chem. 95 (1991) 5031–5041.
[17] S. Matsuo, N. Sakaguchi, H. Wakita, Anal. Sci. 21 (2005) 805–809.
[18] J. Wong, F.W. Lytle, R.P. Messmer, D.H. Maylotte, Phys. Rev. B 30 (1984) 5596–5610.
[19] G. Giuli, E. Paris, J. Mungall, C. Romano, D. Dingwell, Amer. Mineral. 89 (2004) 1640–1646.
[20] A. Walter, R. Herbert, C. Hess, T. Ressler, Chem. Central J. 4 (2010) 3 (20).
[21] R.H. French, H. Müllejans, D.J. Jones, J. Am. Ceram. Soc. 81 (1998) 2549–2557.
[22] A. Kudo, K. Omori, H. Kato, J. Am. Chem. Soc. 121 (1999) 11459–11467.
[23] R. Konta, H. Kato, H. Kobayashi, A. Kudo, Phys. Chem. Chem. Phys. 5 (2003) 3061–3065.
[24] G. Xiao, X. Wang, D. Li, X. Fu, J. Photochem. Photobiol. A: Chem. 193 (2008) 213–221.